4 Digital Holographic Interferometry (DHI)

4.1 General Principles

A conventional holographic interferogram is generated by superposition of two waves, which are scattered from an object in different states. The interferogram carries the information about the phase change between the waves in form of dark and bright fringes. However, as described in chapter 2.7, the interference phase cannot be extracted unambiguously from a single interferogram. The interference phase is usually calculated from three or more phase shifted interferograms by phase shifting algorithm. This requires additional experimental effort.

Digital Holography allows a completely different way of processing [128]. In each state of the object one digital hologram is recorded. Instead of superimposing these holograms as in conventional HI using photographic plates, the digital holograms are reconstructed separately according to the theory of chapter 3. From the resulting complex amplitudes $\Gamma_1(\xi,\eta)$ and $\Gamma_2(\xi,\eta)$ the phases are calculated:

$$\varphi_1(\xi,\eta) = \arctan\frac{\mathrm{Im}\,\Gamma_1(\xi,\eta)}{\mathrm{Re}\,\Gamma_1(\xi,\eta)} \tag{4.1}$$

$$\varphi_2(\xi,\eta) = \arctan\frac{\mathrm{Im}\,\Gamma_2(\xi,\eta)}{\mathrm{Re}\,\Gamma_2(\xi,\eta)} \tag{4.2}$$

The index 1 denotes the first state, the index 2 is for the second state. In Eq. (4.1) and (4.2) the phase takes values between $-\pi$ and π, the principal values of the arctan function. The interference phase is now calculated directly by subtraction:

$$\Delta\varphi = \begin{cases} \varphi_1 - \varphi_2 & \text{if } \varphi_1 \geq \varphi_2 \\ \varphi_1 - \varphi_2 + 2\pi & \text{if } \varphi_1 < \varphi_2 \end{cases} \tag{4.3}$$

This equation permits the calculation of the interference phase modulo 2π directly from the digital holograms. The generation and evaluation of an interferogram is not necessary.

The scheme of Digital HI is shown in figure 4.1. The upper left and upper right figures present two digital holograms, recorded in different states. Between the two recordings the knight has been tilted by a small amount. Each hologram is reconstructed separately by a numerical Fresnel transform. The reconstructed phases according to Eq. (4.1) and (4.2) are depicted in the two figures of the middle row.

The phases vary randomly due to the surface roughness of the object. Subtraction of the phases according to Eq. (4.3) results in the interference phase, lower left figure.

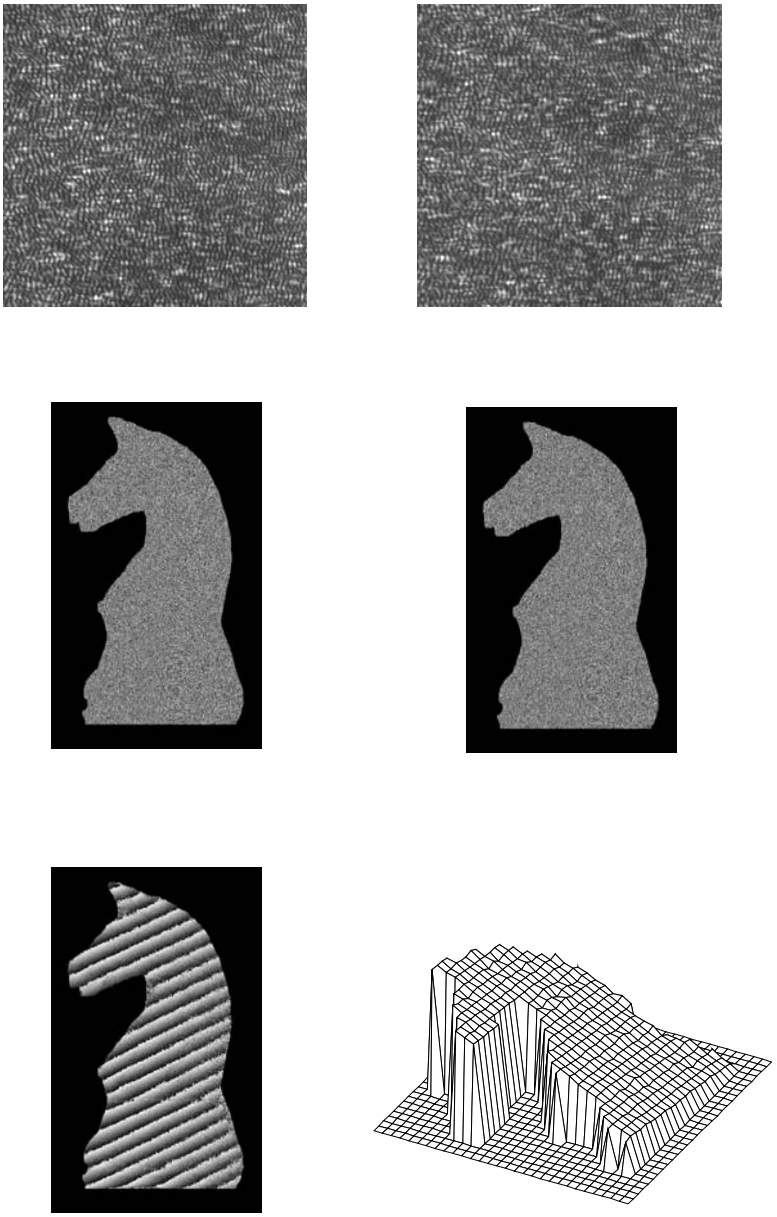

Fig. 4.1. Digital Holographic Interferometry

The interference phase is indefinite to an additive multiple of 2π, i. e. it is wrapped modulo 2π. The information about the additive constant is already lost in the holographic interferometric process. This is not a special property of Digital HI, but also the case for all interferometric methods using the wavelength as a length unit. To convert the interference phase modulo 2π into a continuous phase distribution, one can apply the standard phase unwrapping algorithm developed for conventional interferometry, HI or ESPI. In this example a simple path dependent unwrapping algorithm, as described in chapter 2.7.6, has been applied. The unwrapped phase image is shown in the lower right picture of figure 4.1. The sensitivity vector used for hologram recording is nearly constant and perpendicular over the whole surface. The grey values of the unwrapped phase map can be converted therefore directly into displacement values via Eq. (2.86), i. e. the plot in the lower right picture of figure 4.1 is the object displacement.

4.2 Deformation Measurement

4.2.1 Quantitative Displacement Measurement

As discussed in chapter 4.1 the way to obtain the interference phase in DHI is totally different from conventional HI using photographic recording media and optical reconstruction. On the other hand the derivation of the relation between displacement vector $\vec{d}$, geometrical boundary conditions described by the sensitivity vector $\vec{S}$ and interference phase $\Delta\varphi$ is also valid for DHI. That means the deformation is calculated by Eq. (2.84), which is repeated here:

$$\Delta\varphi(x,y) = \frac{2\pi}{\lambda}\vec{d}(x,y,z)\left(\vec{b}-\vec{s}\right) = \vec{d}(x,y,z)\vec{S} \tag{4.4}$$

As an example for quantitative displacement measurement the deformation of a plate due to impact loading is discussed [134, 139]. The plate is made of fibre reinforced plastic (FRP), which is used more and more in aircraft industry. The deformation behaviour of FRP under impact load differs from that of static loading, so impact experiments are necessary. DHI is well suited to measurement of such transient deformations, because only one single recording is necessary in each deformation state.

The holographic set-up is shown in figure 4.2. The dimensions of the plate are 12cm × 18cm. The recording distance would be too long for direct recording. The spatial frequency spectrum is therefore reduced by a lens, as explained in chapter 3.4.4 (set-up in figure 3.20).

The plate is clamped at three sides by a stable frame. A pneumatically accelerated steel projectile hits the plate and causes a transient deformation. Two holograms are recorded: The first exposure takes place before the impact, when the plate is in rest. The second hologram is recorded 5 microseconds after the impact.

The holograms are recorded by a pulsed ruby laser with a pulse duration of about 30ns, short enough for hologram recording of dynamic events. The second hologram recording is triggered by a photoelectric barrier, which generates the start signal for the laser after the projectile has crossed. The time interval between the impact and the second laser pulse is adjustable by an electronic delay.

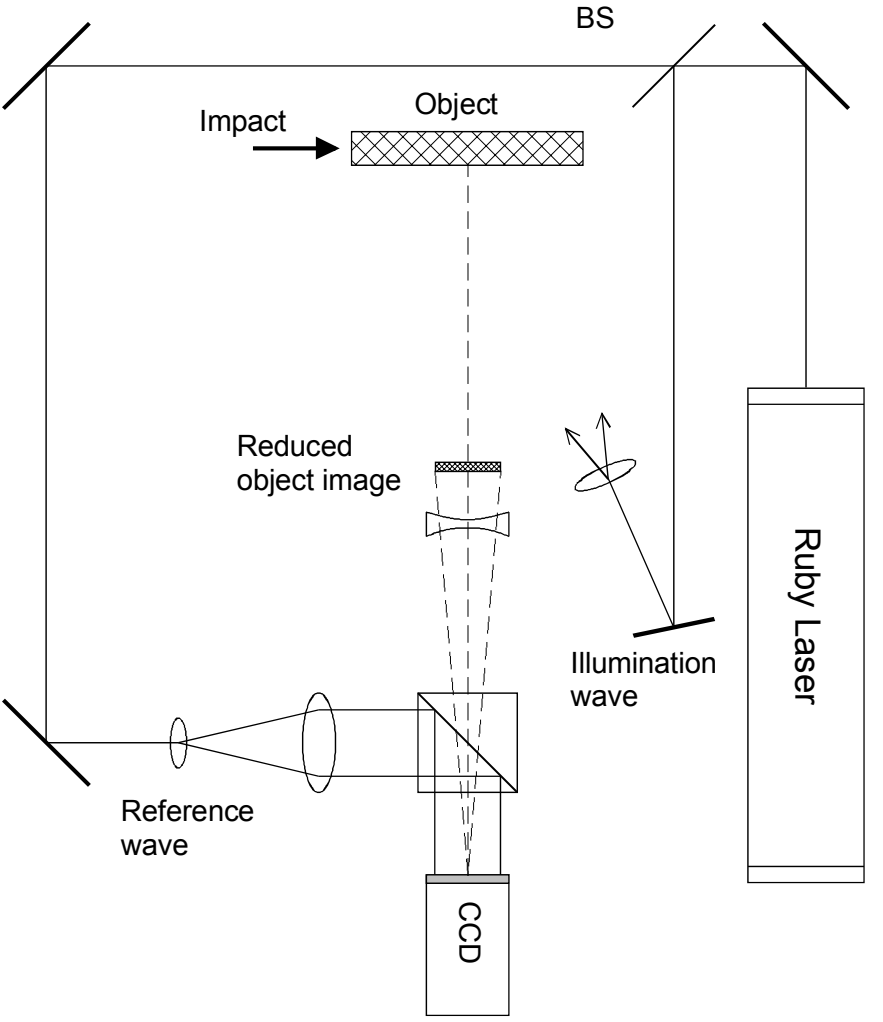

Fig. 4.2. Measurement of transient deformations

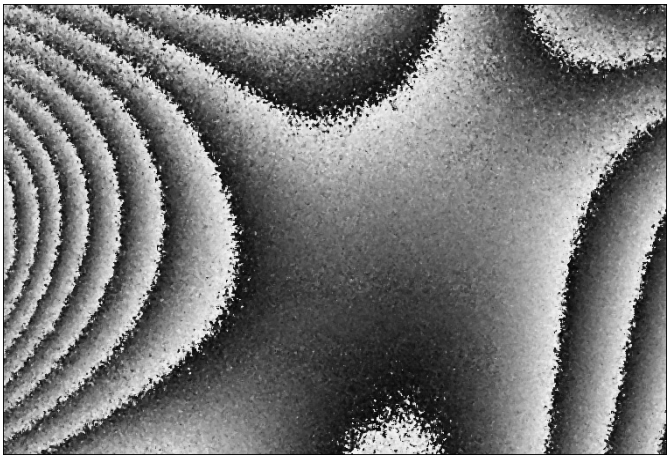

Fig. 4.3. Interference phase modulo 2π

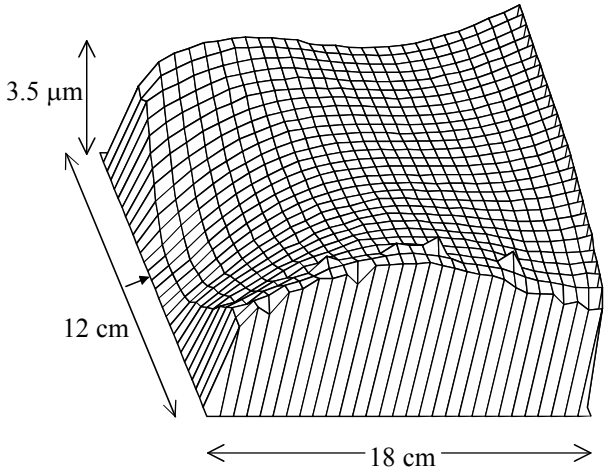

Fig. 4.4. Unwrapped phase, corresponding to deformation 5µs after the impact

Both holograms are reconstructed separately as described in chapter 3. The interference phase map is then calculated by subtracting the reconstructed phase distributions according to Eq. (4.3).

As a typical result, the interference phase modulo 2π and the unwrapped phase are shown in figures 4.3 and 4.4. Since the sensitivity vector is nearly perpendicular to the surface, the unwrapped phase corresponds to the deformation field in z-direction 5µs after the impact.

4.2.2 Mechanical Materials Properties

Digital holographic displacement measurement can used to determine mechanical and thermal material properties such as the Young's modulus, the Poisson ratio and the thermal expansion coefficient. For the derivation of these quantities a procedure for the evaluation of the three-dimensional shape and the three-dimensional displacement of the object under test, a physical model of the behavior of the loaded object and the knowledge about the applied load are necessary. Such a measurement procedure based on DHI has been realized [144]. The physical model must contain one or more of the material constants as parameters. A numerical fit into the measured data according to the physical model delivers the wanted parameters within an accuracy that is determined by the numerical reliability of the model. An outline of the complete evaluation process is shown in figure 4.5 (DHI shape measurement is explained in chapter 4.3).

The calculation of the above mentioned material quantities requires to measure the whole three-dimensional displacement vector field. As stated in chapter 2.7 at least 3 interferograms of the same surface with linear independent sensitivity vectors are necessary. The interferometer consists of an optimized arrangement with 4 illumination directions and 1 observation direction to measure the 3D-displacements and coordinates precisely, figure 4.6. It includes a CCD-camera, a laser, a beam splitter cube to guide the reference beam to the CCD target and some optics for beam shaping. Optionally, a fibre coupler can be included to switch several illumination directions for varying the sensitivity vector. Such an interferometer can be designed in a very compact way, figure 4.6. Micro silicon beams are used as test samples, figure 4.7.

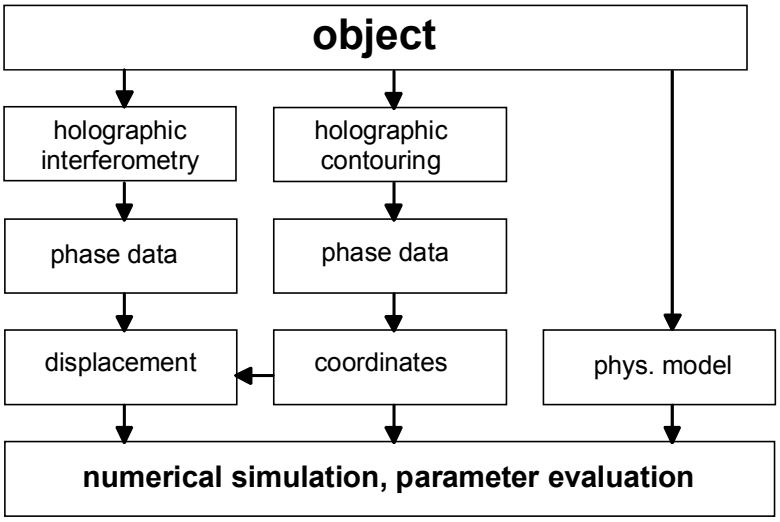

Fig. 4.5. Evaluation scheme for material properties

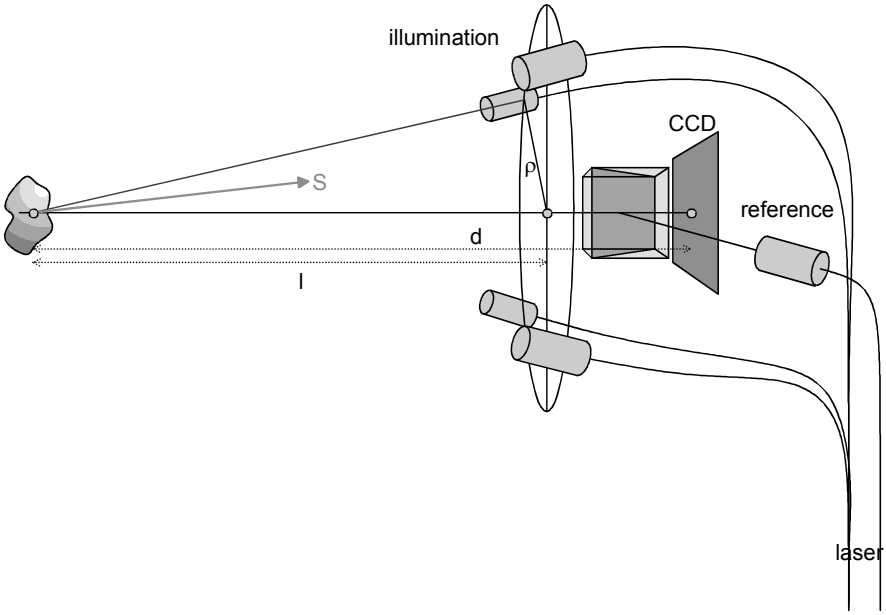

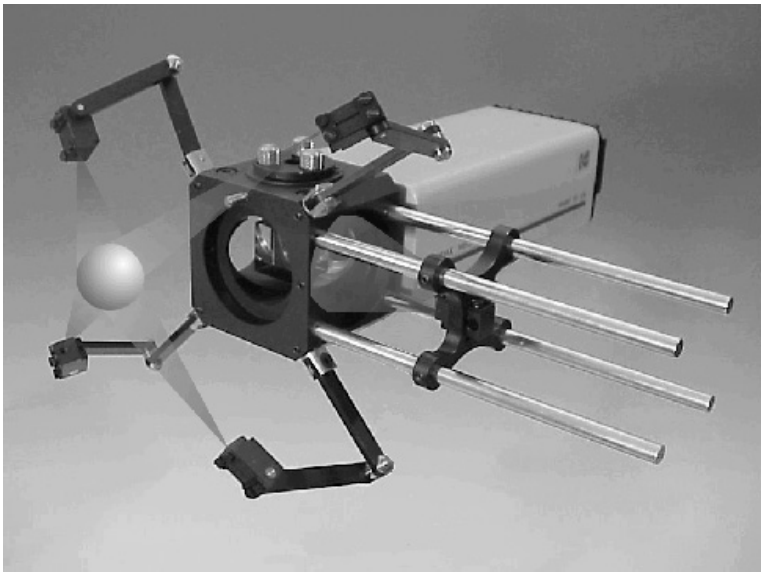

Fig. 4.6. DHI set-up with four illumination directions (top) and its practical implementation (bottom, photo: BIAS)

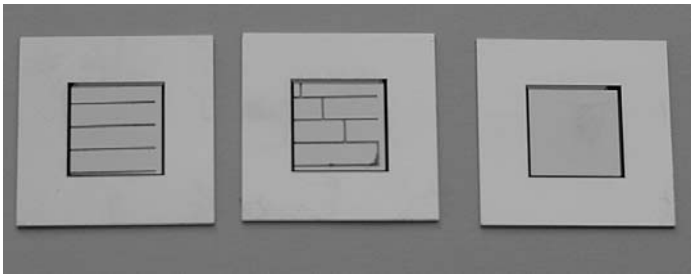

Fig. 4.7. Test samples made on 100mm diameter silicon wafer. The size of the quadratic structure is 9mm × 9mm, the thickness of the components is between 10μm and 40μm.

The first example is the determination of the Poisson ratio by DHI. Moments of force are applied to a rectangular sample at opposite sides. Fig. 4.8a shows a typical loading machine designed especially for small objects. The small dimensions of the samples demand a precise adjustment of all components: the "chop" which pushes against the object from above, the support and the sample which has the shape of a small rectangular beam. In this way a homogeneous deformation is achieved. Unwanted torsions of small magnitude are corrected numerically. This can be done easily with the use of the mod 2π-phase maps from Digital Holography. The resulting deformation is recorded and evaluated. The deflection causes hyperbolic structures in the 2π-phase map, figure 4.8b. Conventionally, the Poisson ratio is derived numerically from the angle between the asymptotic lines of the fringes of equal phase [170]. The deformation can be formulated by the following equation in first order approximation:

$$u(y,z) = -\frac{1}{2R}\left[z^2 + \nu\left(a^2 - y^2\right)\right] \tag{4.5}$$

Here u means the deformation in x-direction at position (y,z) on the surface of the object. ν stands for the Poisson ratio. R is the radius of curvature and a is a constant parameter. R results from a slight deflection in the initial state. This helps to ensure a proper mechanical contact between the support and the sample. Eq. (4.5) shows that the upper and lower surface of the sample are deformed to parabolic curves where the inside is bent in a convex way and the outside is curved in a concave way. Since this analytical model contains the Poisson ratio as a parameter it is possible to use the measured deformation for its evaluation. This is performed numerically by approximating the model to the data (figure 4.8c) with a least-square-fit, figure 4.8d.

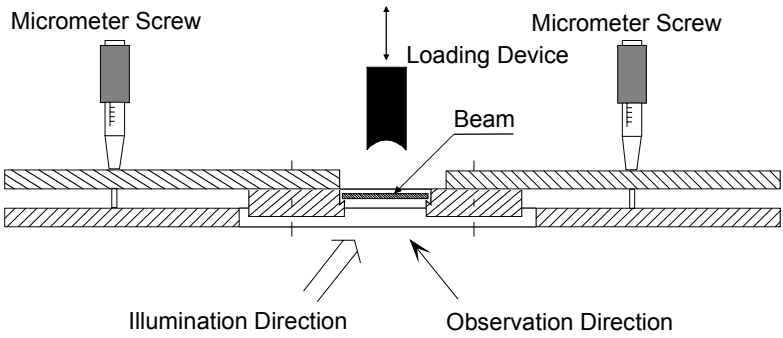

a) Schematic experimental set-up

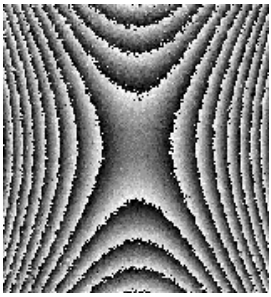

b) Reconstructed mod 2π-phase map

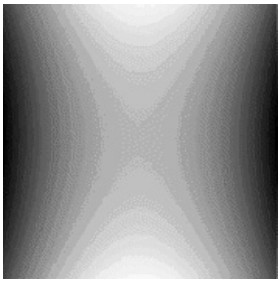

c) Unwrapped phase field

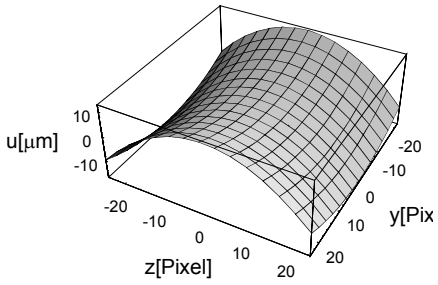

d) Approximated function

Fig. 4.8. Measurement of the Poisson ratio by DHI (from [144])

The reproducibility and accuracy of the values obtained by this method is good in comparison to conventional optical techniques for small samples. Table 4.1 contains some of the results for beams made of spring steel, structural steel and titanium. The values correlate with the values given by the manufacturers within the tolerances of the material batches.

Table 4.1. Measured Poisson ratios compared with literature values

Material	Width [mm]	Thickness [mm]	Length [mm]	Poisson Ratio measured	Poisson Ratio literature
Spring steel	1.20	0.20	12.0	0.288	0.29-0.31
Spring steel	2.00	0.10	12.0	0.301	0.29-0.31
Structural steel	1.00	0.50	10.0	0.338	0.29-0.31
Structural steel	1.50	0.50	10.0	0.345	0.29-0.31
Titanium	2.00	0.80	10.0	0.359	0.361
Titanium	1.00	0.80	10.0	0.381	0.361

The Young's modulus can be determined in a similar way as the Poisson ratio if the physical model contains this quantity as a parameter. Small silicon beams which are clamped at one edge and mechanically loaded at the opposite edge with a defined force are used. The 3D-surface displacement (u,v,w) (Fig. 4.9c) can be measured with the interferometer by evaluating at least 3 interferograms (Fig. 4.9b) made with different illumination directions. A model of the beam bending containing the Young's modulus E as a free parameter is the basis for a numerical fit of the experimental values:

$$u(y) = \frac{Fl^3}{6EI_y}\left(2 - 3\frac{y}{l} + \frac{y^3}{l^3}\right) \tag{4.6}$$

u is the displacement in x-direction and y a position on the beam of the length l. I_y is the axial moment of inertia in the *(x,z)*-plane that can be estimated with the help of a shape measurement. F is the force applied to the tip of the beam. The applied forces are relatively small so that a special loading mechanism was developed, Fig. 4.9a. The spring constant k is assumed to be known precisely as well as the displacement $\Delta a = a - a'$. With this information the force can be evaluated with the equation

$$F = k\Delta a \tag{4.7}$$

Several experiments with thin beams made of silicon (dimensions: length 3mm, width 1mm) delivered an average value of E=162MPa. The literature value (in the considered crystal direction) is about 166MPa. These values can vary in a big range according to the material's history, treatment and degree of impurity.

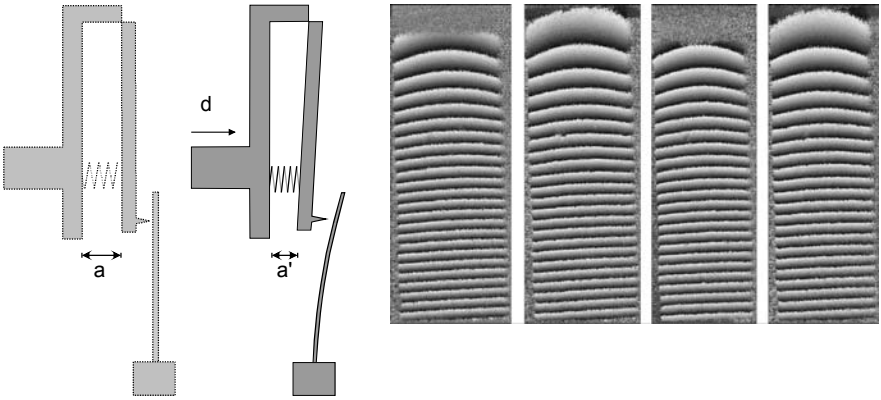

a) working principle of the loading mechanism for the small samples

b) four 2π-phase maps recorded from four different illumination directions

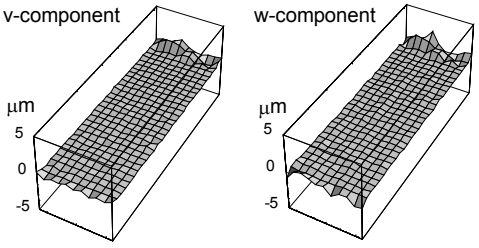

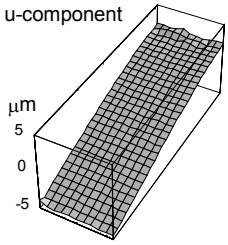

c) deformation calculated in cartesian coordinates (scale of the plots in μm)

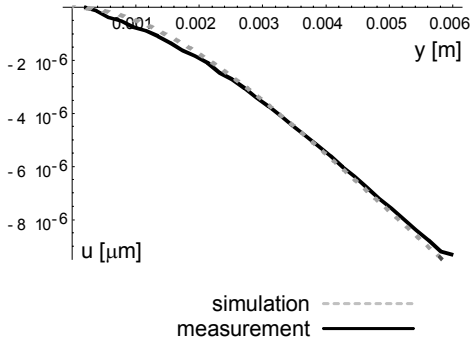

d) profile of the deformation in x-direction

Fig. 4.9 Determination of Young's modulus by DHI

4.2.3 Thermal materials properties

DHI is applied also to measure thermal materials properties, e. g. the thermal expansion coefficient. For interferometric investigations of the thermal behavior it must be ensured that thermal turbulences and non-uniform temperature distributions are avoided. Therefore a vacuum chamber is used that can be supplied with adapted loading devices, figure 10a. The thermal loading device is capable of keeping a constant temperature within an accuracy of 0.02°C in a range of about 20°C up to 180°C, figure 4.10b. The digital holographic interferometer is mounted outside at the observation window of the chamber, figure 4.10c.

A mono-crystal silicon beam (figure 4.10d) with phosphor coating is used as a test object. The interferograms are recorded at various temperature differences. The complete evaluation process can be summarized as follows:

- the geometry of the setup is measured to get the geometry matrix for the evaluation of the 3 displacement components
- 4 holograms are recorded in the initial state of the object
- the object is loaded thermally and recorded holographically from four different illumination directions
- the displacement vector components *(u,v,w)* are calculated based on the evaluation of the 4 2π-phase maps
- rigid body motions were separated from internal deformations of the object itself by subtracting the mean movement from the displacement values.
- the absolute length change ΔL is determined as well as the total length of the beam which can be performed by using the imaging properties of Digital Holography. The thermal expansion coefficient in y- and z-direction can simply be calculated by using the equation

$$\alpha = \frac{\Delta L}{L_0 \Delta T} \tag{4.8}$$

The extension in x-direction is too small to be detected with the method applied.

As an example the thermal expansion coefficient α of a small 2mm x 9mm x 100µm mono-crystal silicon beam has been measured. Fig. 4.11 shows the four resulting 2π-phase maps. The applied temperature difference ΔT is 30°C. After elimination of the rigid body motion the three deformation components are evaluated as shown in Fig. 4.12. Considering the dimensions of the beam a value for α of about $\alpha = 2.92 \times 10^{-6}\, 1/K$ results. The literature values vary in a big range due to different measurement methods, conditions and material batches: $\alpha = 2.4...6.7 \times 10^{-6}\, 1/K$.

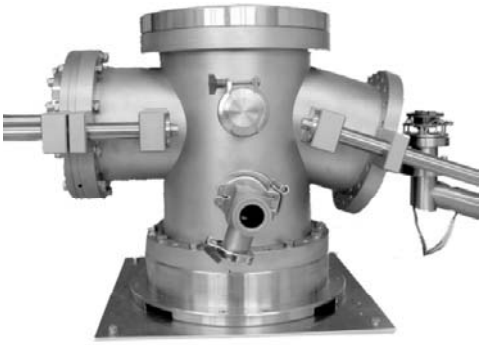

a) Vacuum chamber with the supply channel

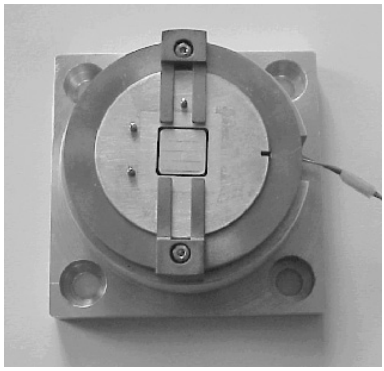

b) Equipment for thermal loading

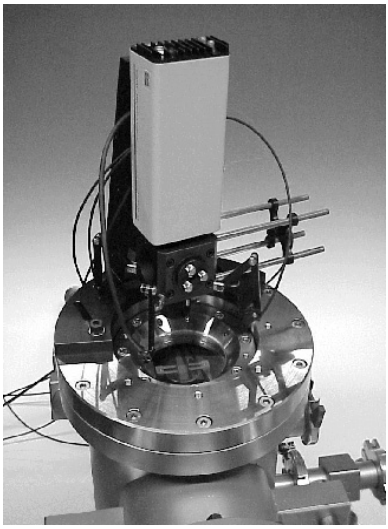

c) Interferometer mounted on the inspection window

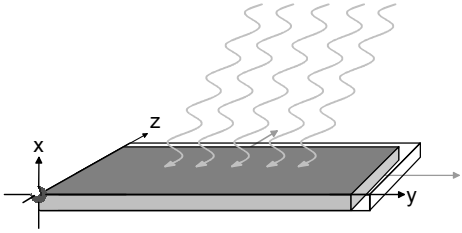

d) coordinate system used for the calculation of the thermal expansion coefficient

Fig. 4.10. Determination of the thermal expansion coefficient by DHI (photos: BIAS)

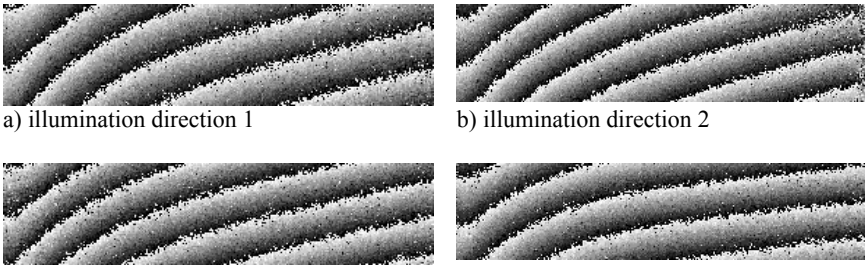

a) illumination direction 1 b) illumination direction 2

c) illumination direction 3 d) illumination direction 4

Fig. 4.11. 2π-phase maps due to deformation by thermal loading, four different illumination directions

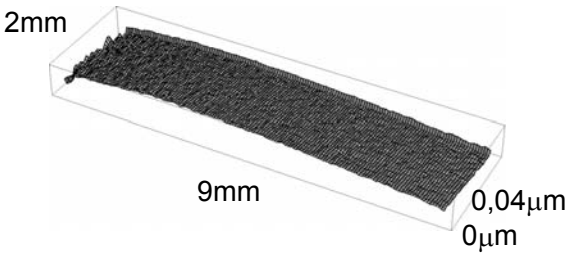

a) u-component

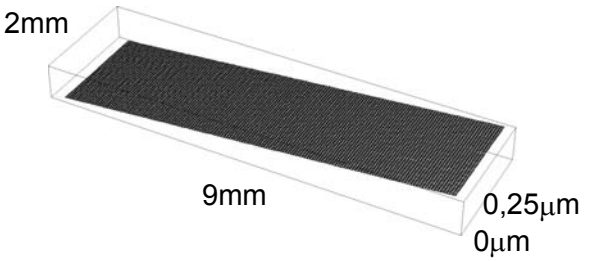

b) v-component

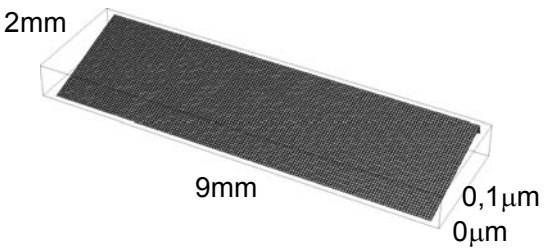

c) w-component

Fig. 4.12. 3D-displacement vector components (u,v,w) of thermally loaded object

4.2.4 Non-Destructive Testing

Non-Destructive Testing (NDT) is used to test materials and components without destruction. NDT methods are applied e. g. in aircraft industry, in power plants and in automotive production. Several physical techniques exist for NDT: Ultrasonic testing, eddy current measurements, penetrant testing, x-ray and also optical methods like HI, ESPI and shearography.

Holographic Non-Destructive Testing (HNDT) measures the deformation due to mechanical or thermal loading of a specimen. Flaws inside the material are detected as an inhomogeneity in the fringe pattern corresponding to the surface deformation.

HNDT can be used wherever the presence of a structural weakness results in a surface deformation of the stressed component. The load can be realized by the application of a mechanical force or by a change in pressure or temperature. Holographic NDT indicates deformations down to the submicrometer range, so loading amplitudes far below any damage threshold are sufficient to produce detectable fringe patterns.

In HNDT it is sufficient to have one fringe pattern of the surface under investigation. Quantitative evaluation of the displacement vector field is usually not required. The fringe pattern is evaluated qualitatively by the human observer or, more and more, by fringe analysis computer codes. Irregularities in the interference pattern are indicators of flaws within the component under investigation.

As discussed in the preceding chapters, DHI generates not a fringe pattern, but directly the interference phase map. This phase map is therefore used for flaw detection in Digital Holographic Non-Destructive Testing (DHI NDT).

As an application for DHI NDT testing of a pressure vessel [138] is described. Such vessels are used as gas tanks in satellites, see figure 4.13. The diameter is in the order of 1 or 2 meter and the thickness of the wall in only about 1 millimetre. Typical flaws to be detected are cracks or reduced thickness of the wall.

The surface of the tank is divided into segments of about $5cm \times 5cm$. For each segment, a series of digital holograms is recorded. Between the exposures, the pressure inside the tank is varied by a few hundred hPa. As a typical result the interference phase between one pair of holograms is shown in figure 4.14. The disturbance in the middle is an indication for a flaw. The interference phase can also be converted into a continuous phase by unwrapping the 2π-jumps. However, for flaw detection the unwrapped phase map is often more suitable.

In conventional holographic NDT the load applied to the object under investigation is restricted to certain limit. Loads above this limit lead to irresolvable fringe densities. In the numerical reconstruction process of DHI, the phase difference between any pair of exposures can be calculated. Even if the total deformation between the first and the last hologram is too high for direct evaluation, the total phase difference can be calculated step by step as the sum of the individual phase changes:

$$\Delta\varphi_{total} = \Delta\varphi_{1\to 2} + \Delta\varphi_{2\to 3} + \Delta\varphi_{3\to 4} + \ldots \tag{4.9}$$

However, a drawback of DHI compared to conventional HI shall be emphasized: For visual flaw detection it is sometimes of advantage to vary the observation direction continuously (dynamic evaluation). This is possible for holograms recorded on a photographic plate with dimensions of about $10cm \times 10cm$ or more, but until now not for digital holograms recorded by a CCD with only about $1cm \times 1cm$ area. However, future progress in camera technology and computer hardware may solve this problem.

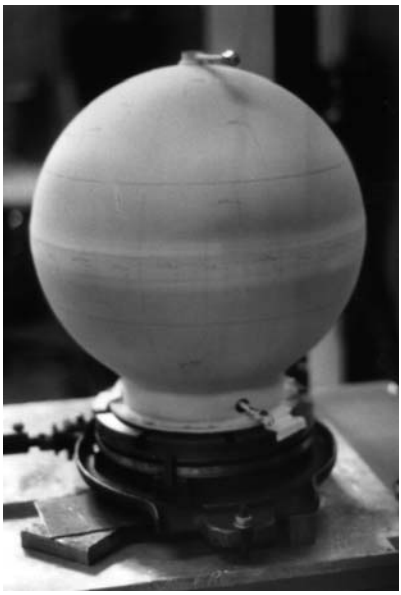

Fig. 4.13. Satellite tank

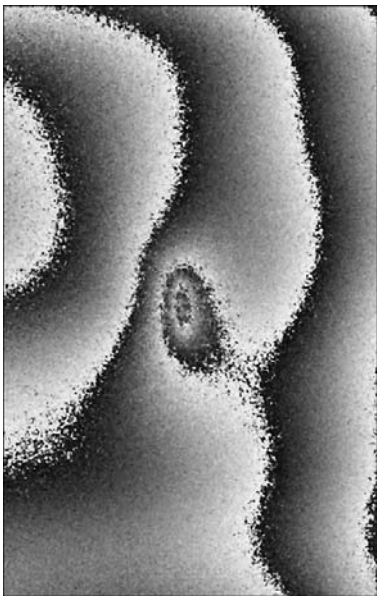

Fig. 4.14. Non-destructive testing by DHI

4.3 Shape Measurement

4.3.1 Two-Illumination-Point Method

The two contouring techniques discussed in chapter 2.7.3 for conventional HI are also applied in DHI.

For the Two-Illumination-Point method it is necessary to record two digital holograms of the same surface, but with different object illumination points. Both holograms are reconstructed separately. The interference phase map, which represents the object shape, is then calculated by subtracting the individual phase distributions according to Eq. (4.3). The result is a wrapped phase map, which is in-

terpreted similar to the contour fringe pattern discussed in chapter 2.7.3. The phase change between two adjacent 2π-jumps is

$$\Delta\varphi = \frac{2\pi}{\lambda}\vec{p}\vec{s} \tag{4.10}$$

with $\vec{p}$ and $\vec{s}$ as defined previously. By analogy with Eq. (2.96) the distance between two adjacent 2π-jumps is

$$\Delta H = \frac{\lambda}{2\sin\frac{\theta}{2}} \tag{4.11}$$

where θ is the angle between the two illumination directions.

DHI two-illumination-point contouring can be carried out e. g. with the set-up depicted in figure 4.15. Optical fibres are preferably used to guide the illumination wave. The fibre output is the illumination source point. The shift is realized e. g. by a motor driven translation stage. The first digital hologram is recorded with the fibre end at position S. For the second hologram the fiber is shifted slightly to position S'.

In order to obtain a maximum sensitivity in a direction normal to the surface, the illumination should come from the side, i. e. the angle between illumination direction and observation direction is near 90°. Still, a such flat illumination directions may cause shadows due to surface variations. The optimum illumination direction is therefore always a compromise between maximum sensitivity and minimum shadows in the reconstructed images.

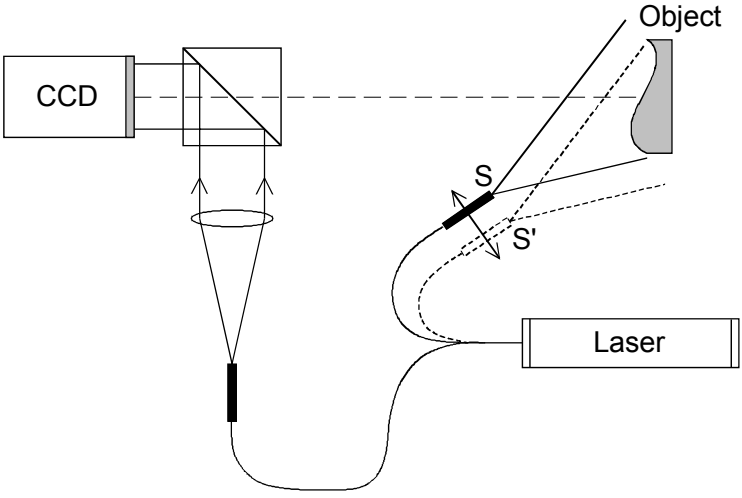

Fig. 4.15. Two-illumination point DHI

4.3.2 Two- and Multi-Wavelength Method

For shape measurement by the two-wavelength method two holograms are recorded with different wavelengths λ_1 and λ_2. In conventional HI both holograms are recorded on a single photographic plate. Both holograms are reconstructed by the same wavelength, e. g. λ_1. That is why two images of the object are generated. The image recorded and reconstructed by λ_1 is an exact duplicate of the original object surface. The image which has been recorded with λ_1, but is reconstructed with λ_2 is slightly shifted in observation direction (towards the observer, see imaging equations in chapter 2.6.2) with respect to the original surface. These two reconstructed images interfere.

The concept of two-wavelength contouring has been introduced into Digital Holography, too [62, 129, 143]. Two holograms are recorded with λ_1 and λ_2 and stored electronically, e. g. with the set-up depicted in figure 4.16. In contrast to conventional HI using photographic plates, both holograms can be reconstructed separately by the correct wavelengths according to the theory of chapter 3. From the resulting complex amplitudes $\Gamma_{\lambda 1}(\xi,\eta)$ and $\Gamma_{\lambda 2}(\xi,\eta)$ the phases are calculated:

$$\varphi_{\lambda 1}(\xi,\eta) = \arctan \frac{\mathrm{Im}\,\Gamma_{\lambda 1}(\xi,\eta)}{\mathrm{Re}\,\Gamma_{\lambda 1}(\xi,\eta)} \tag{4.12}$$

$$\varphi_{\lambda 2}(\xi,\eta) = \arctan \frac{\mathrm{Im}\,\Gamma_{\lambda 2}(\xi,\eta)}{\mathrm{Re}\,\Gamma_{\lambda 2}(\xi,\eta)} \tag{4.13}$$

As for deformation analysis the phase difference is now calculated directly by subtraction:

$$\Delta\varphi = \begin{cases} \varphi_{\lambda 1} - \varphi_{\lambda 2} & if \varphi_{\lambda 1} \geq \varphi_{\lambda 2} \\ \varphi_{\lambda 1} - \varphi_{\lambda 2} + 2\pi & if \varphi_{\lambda 1} < \varphi_{\lambda 2} \end{cases} \tag{4.14}$$

This phase map is equivalent to the phase distribution of a hologram recorded with the synthetic wavelength Λ. In conventional two-wavelength contouring the distance between adjacent fringes corresponds to a height step of $\Lambda/2$, see Eq. (2.90). Similarly in two-wavelength DHI a 2π phase jump corresponds to a height step of $\Lambda/2$:

$$\Delta H = \frac{\lambda_1 \lambda_2}{2|\lambda_1 - \lambda_2|} = \frac{\Lambda}{2} \tag{4.15}$$

A typical example of two-wavelength contouring is shown in figure 4.17.

In DHI contouring both holograms are reconstructed with the correct wavelength. Distortions resulting from hologram reconstruction with a different wavelength than the recording wavelength, as in conventional HI contouring, are therefore avoided.

A modified contouring approach, which is referred to as *multiwavelength contouring*, has to use more than two illumination wavelengths to eliminate ambiguities inherent to modulo 2π phase distributions [66, 67, 110, 163]. The advantage of this technique is that it can also be used with objects that have phase steps or isolated object areas.

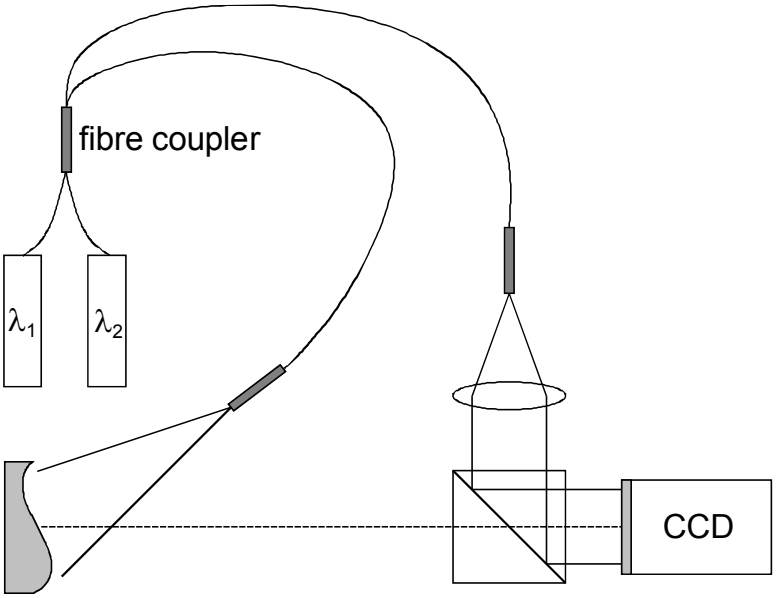

Fig. 4.16. Two-wavelength DHI

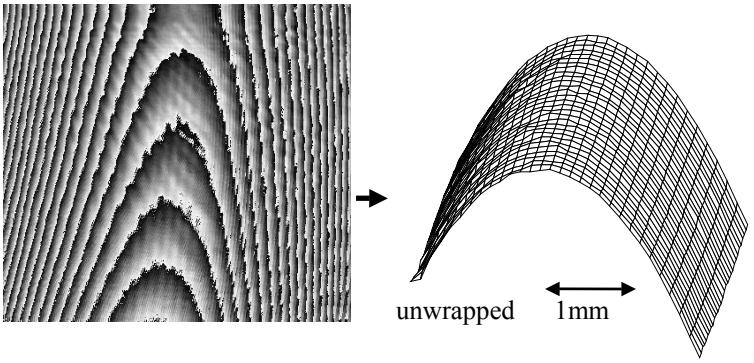

Fig. 4.17. Shape registration of a cylindrical lens by two-wavelength contouring. Visible part: 3mm × 2mm

4.3.3 Hierarchical Phase Unwrapping

As stated earlier the process of phase unwrapping is always the same for conventional HI as well as for DHI and in general also for all methods which generate modulo 2π images. In chapter 2.7.6 a simple phase unwrapping method is described. However, for DHI multiwavelength contouring a special unwrapping procedure named *hierarchical phase unwrapping* is useful. The basic idea of this technique was originally developed by Nadeborn and Osten for projected fringe techniques with incoherent light [99, 107], but it is applicable for all measurement techniques which generate periodic data. *Hierarchical phase unwrapping* is particularly well suited in conjunction with DHI multi-wavelength contouring. The technique is discussed in this context.

The practical application of interferometric contouring techniques leads to following problems [142]:

- Fringe counting problem: The interference phases are periodic. For the Two-Wavelength method the periodic length is half the synthetic wavelength, see Eq. (4.15). If edges, holes, jumps or other discontinuations are on the measured surface, it is often not possible to count the absolute interference order, resp. phase value. An unambiguous evaluation is not possible. In order to generate unambiguous results, it is therefore necessary to use a synthetic wavelength bigger than twice the maximum height variation of the object. But this causes the second problem:
- Noise problem: The phase noise of the measurement increases the larger the synthetic wavelength gets. A large synthetic wavelength, necessary to generate unambiguous phase values, often leads to larger phase noise. To measure e. g. the surface profile of an object with about 10mm height variations, a synthetic wavelength of at least $\Lambda = 20mm$ is necessary. In practice the phase noise limits the achievable measurement resolution to about 1/10 of the synthetic wavelength; i. e. the accuracy of the measured height data is only 0.2mm. This is too low for many applications.

The basic idea of hierarchical phase unwrapping is to start with a large synthetic wavelength to avoid phase ambiguities [163]. This measurement is not very accurate due to noise. The accuracy is now improved by systematic reduction of the synthetic wavelengths, while the information of the preceding measurements is used to eliminate ambiguities.

The procedure starts with a synthetic wavelength Λ_1, which is larger than twice the maximum height variation of the object. The height at a certain position is then given by

$$z_1 = \frac{\Lambda_1}{2}\frac{\Delta\varphi_1}{2\pi} \tag{4.16}$$

where $\Delta\varphi_1$ is the measured interference phase at this position. This result is unambiguous, but strongly disturbed by noise. Now the synthetic wavelength is

reduced to Λ_2 and a new phase measurement is made. The resulting height coordinate

$$\hat{z}_2 = \frac{\Lambda_2}{2}\frac{\Delta\varphi_2}{2\pi} \tag{4.17}$$

is not unambiguous, this is indicated by the "^". In the next step the difference between the result of the first measurement z_1 and the second measurement $\hat{z}_2$ is calculated:

$$\Delta z = z_1 - \hat{z}_2 \tag{4.18}$$

Furthermore it is calculated which multiple of the periodic length $\Lambda_2/2$ is contained in the difference Δz (rounded number):

$$N = floor\left(2\frac{\Delta z}{\Lambda_2} + 0.5\right) \tag{4.19}$$

The function $f(x) = floor(x)$ delivers the maximum integer value, which is smaller than *x*. The correct result of the second measurement is now:

$$z_2 = \hat{z}_2 + \frac{\Lambda_2}{2}N \tag{4.20}$$

This result is unambiguous as well as z_1, but it has a better accuracy compared to z_1 due to the smaller synthetic wavelength. The procedure is continued with smaller wavelengths as long as the resolution is below a desired value. After *n* iterations one gets the formula:

$$z_n = \hat{z}_n + \frac{\Lambda_n}{2}\,floor\left(2\frac{z_{n-1} - \hat{z}_n}{\Lambda_n} + 0.5\right) \tag{4.21}$$

In practice the number of measurements to reach the desired resolution should be as small as possible. This minimum or optimum number depends on the noise. Let ε_n be the inaccuracy in a measurement using the synthetic wavelength Λ_n. The true height coordinate z_{true} lies within an interval limited by

$$\begin{aligned} z_{\max} &= z_{meas} + \frac{\varepsilon_n}{2}\frac{\Lambda_n}{2} \\ z_{\min} &= z_{meas} - \frac{\varepsilon_n}{2}\frac{\Lambda_n}{2} \end{aligned} \tag{4.22}$$

where z_{meas} is the value determined by the measurement. Then the next measurement with Λ_{n+1} takes place. The inaccuracy of this measurement is given by

ε_{n+1}. Now the noise of the nth and the (n+1)th measurement is considered for estimating the interval limits of the true height coordinate:

$$z_{\max} = z_{meas} + \frac{\varepsilon_n}{2}\frac{\Lambda_n}{2} + \frac{\varepsilon_{n+1}}{2}\frac{\Lambda_{n+1}}{2} \qquad (4.23)$$
$$z_{\min} = z_{meas} - \frac{\varepsilon_n}{2}\frac{\Lambda_n}{2} - \frac{\varepsilon_{n+1}}{2}\frac{\Lambda_{n+1}}{2}$$

The difference between the maximum possible and the minimum possible height coordinate is:

$$\left|z_{\max} - z_{\min}\right| = \varepsilon_n \frac{\Lambda_n}{2} + \varepsilon_{n+1}\frac{\Lambda_{n+1}}{2} \qquad (4.24)$$

A correct recovery of the absolute height coordinate is only possible, if following condition is satisfied for the (n+1)th measurement:

$$\frac{\Lambda_{n+1}}{2} \geq \left|z_{\max} - z_{\min}\right| \qquad (4.25)$$

A smaller value for $\Lambda_{n+1}/2$ than $\left|z_{\max} - z_{\min}\right|$ would lead to ambiguities, because $\hat{z}_{n+1} + N\Lambda_{n+1}/2$ as well as $\hat{z}_{n+1} + (N+1)\Lambda_{n+1}/2$ are possible height values within the interval limits. The optimum period (half synthetic wavelength) is achieved for the equals sign.

The combination of Eq. (4.24) and (4.25) with the equals sign results to:

$$\Lambda_{n+1} = \Lambda_n \frac{\varepsilon_n}{1-\varepsilon_{n+1}} \qquad (4.26)$$

This condition determines the optimum choice of the sequence of synthetic wavelengths depending on each measurement's accuracy.

4.4 Measurement of Refractive Index Variations

Digital HI is also used to measure refractive index variations within transparent media, e. g. with the set-up of figure 4.18. The expanded laser beam is divided into reference and object beam. The object beam passes the transparent phase object and illuminates the CCD. The reference beam impinges directly on the CCD. Both beams interfere and the hologram is digitally recorded. The set-up is very similar to a conventional Mach-Zehnder interferometer. The difference is that the interference figure here is interpreted as a hologram, which can be reconstructed with the theory of chapter 3. Therefore all features of Digital Holography like direct access to the phase or numerical re-focussing are available.

Just like for deformation analysis two digital holograms are recorded: The first exposure takes place before, and the second after the refractive index change.

These digital holograms are reconstructed numerically. From the resulting complex amplitudes $\Gamma_1(\xi,\eta)$ and $\Gamma_2(\xi,\eta)$ the phases are calculated by Eq. (4.1) and (4.2). Finally the interference phase is calculated by subtraction according to Eq. (4.3).

In the reconstruction of holograms recorded by the set-up of figure 4.18 the undiffracted reference wave, the real image and the virtual image are lying in one line. The images overlap, which causes distortions. The undiffracted reference wave can be suppressed by filtering with the methods discussed in chapter 3.3.1. The overlapping of the unwanted twin image (either the virtual image if one focuses on the real image or vice versa) can be avoided by slightly tilting the reference wave, as discussed in chapter 3.3.2. In this case the images are spatially separated.

The interferometer of figure 4.18 is sensitive to local disturbances due to imperfections in optical components or dust particles. The influence of these disturbances can be minimized if a diffusing screen is placed in front of or behind the phase object. In this case the unfocused twin image appears only as a diffuse background in the images, which does not disturb the evaluation. If a diffuser is introduced no additional tilting of the reference wave is necessary for image separation. A disadvantage of using a diffuser is the generation of speckles due to the rough surface.

In figure 4.19 a typical interference modulo 2 π image of a transparent phase object is shown. The holograms are recorded with the set-up of figure 4.18 (without diffuser). The object volume consists of a droplet of toluene, which is introduced into the liquid phase water/ acetone. The refractive index changes are caused by a concentration gradient, which is induced by the mass transfer of acetone into the droplet.

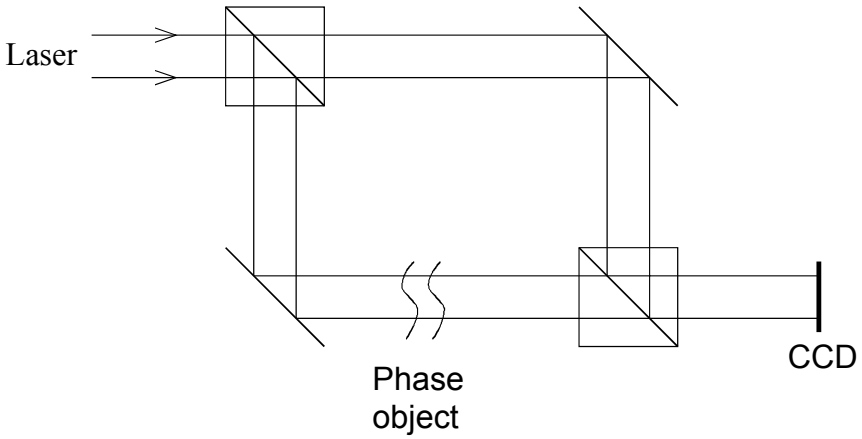

Fig. 4.18. DHI set-up for transparent phase objects

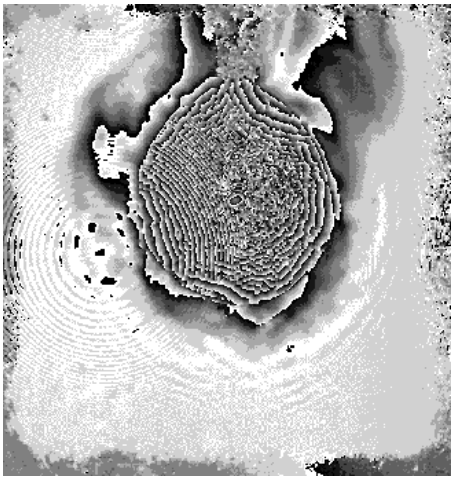

Fig. 4.19. Wrapped phase of a liquid system